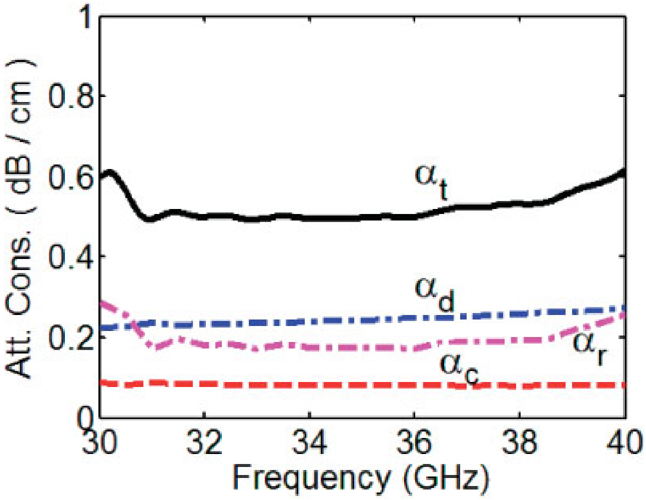


**Figure 6** Attenuation constant versus frequency for proposed structure. [Color figure can be viewed in the online issue, which is available at www.interscience.wiley.com]

ample, by setting GaAs as a lossless substrate, total value of conductor and radiative loss can be obtained. In this way, radiative loss may be extracted from the simulation of perfect conductor and lossless substrate using HFSS software. In Figure 3, dielectric loss is almost constant against frequency and higher radiative loss is observed in high frequencies. Conductor loss has important role in the total loss and increases by frequency. According to the figure, total microwave loss decreases by the microstrip width and thickness of the substrate. The simulated results are in good agreement with the measured results from [4] and [5]. In addition, bandwidth of WGPD which can be limited by microstrip loss is the challenging problem for the high frequency applications.

In Figure 4, electrical fields inside of the structure shown in Figure 2 are illustrated. Figure 4(a) illustrates the microstrip field in the point (A) of Figure 2. In Figure 4(b), quasi-TEM mode is converting to $TE_{10}$ mode in point (B) of Figure 2. Thickness of substrate in the top layer is less than the bottom layer to have a good transition. In Figure 4(c), microwave field which is now pure $TE_{10}$ mode in the middle of structure is illustrated. As shown in Figure 4, the complete conversion from microstrip quasi-TEM mode to SIW $TE_{10}$ mode is done.

Figure 5 shows the measured and simulated results for two back-to-back transitions of the circuit in Figure 2. For the measurement purpose, an HP8510 network analyzer and a Wiltron test fixture were used. Insertion loss of about 1 dB and 2 dB for the simulation and measurement are obtained, respectively. Also, less than $-15$ dB of return loss for the whole frequency range is obtained. As it is shown in the figures, good agreement between the measured and simulated results is observed. The little difference between the results is related to the fabrication precise in SIW width.

In Figure 6, microwave loss analysis for the new proposed structure is shown. The effects of small microstrip parts as WGPD, two transitions of microstrip to SIW and multilayer SIW structure are included in this result. All of losses are almost constant between 30 and 40 GHz. This structure is band-pass device and cutoff frequency of designed SIW is 20 GHz. Microwave losses in SIW structure decrease after $TE_{10}$ cutoff frequency and is almost constant before $TE_{20}$ cutoff frequency [1]. By comparing Figures 3 and 6, one can observe that microstrip conventional waveguide should be replaced with SIW structure for the high frequency applications such as radio over fiber systems.

## 4. CONCLUSION

The new SIWPD has been designed and introduced. Conventional WGPD with microstrip transmission line were analyzed and compared with SIWPD. Also, the microwave characteristics of the new structure including the transition from the microstrip to SIW has been realized and measured. In SIW part, two-layer substrate separate DC-bias of the optoelectronic device and microwave signal. Good agreement between the simulated and measured results for the insertion and return loss are obtained.

## REFERENCES


1. K. Wu, E. Mortazy, and M. Bozzi, Development of microwave and millimeter-wave traveling-wave electro-optical devices using substrate integrated circuit concept, Proc Microwave Photon (2007), 62–65.
2. S.-C. Kong, S.-J. Yoon, and Y.-W. Choi, Microwave characteristics of long TWPDs for high-power operation, Microwave Opt Technol Lett 35 (2002), 51–54.
3. D. Wake, T.P. Spooner, S.D. Perrin, and I.D. Henning, 50 GHz InGaAs edge-coupled PIN photodetector, Electron Lett 27 (1991), 1073–1075.
4. E. Goldfarb and A. Platzker, Losses in GaAs microstrip, IEEE Trans Microwave Theory Tech 38 (1990), 1957–1962.
5. J.P. Thakur, A.K. Pandey, A. Kedar, K.K. Gupta, H.P. Vyas, Modelling of GaAs-MMIC microstrip line up to 40 GHz, Int J RF Microwave Comput-Aided Eng 14 (2004), 475–482.
6. K. Wu, D. Deslandes, and Y. Cassivi, The substrate integrated circuits—A new concept for high-frequency electronics and optoelectronics, In Proceedings of the 6th International Conference on Telecommunications Modern Satellite (2003), pp. 1–10.
7. D. Deslandes and K. Wu, Single-substrate integration technique of planar circuits and waveguide filters, IEEE Trans Microwave Theory Tech 51 (2003), 593–596.
8. Ansoft HFSS version 11, Ansoft Corp., Pittsburgh, PA, 2008.




# A COMPACT TRIPLE-BAND ANTENNA DESIGN FOR UMTS, WLAN AND WIMAX APPLICATIONS


**Jhin-Fang Huang, Ming-Tzan Wu, and Jiun-Yu Wen**

Department of Electronic Engineering, National Taiwan University of Science and Technology, No. 43, Sec. 4, Keelung Rd, Taipei, Taiwan, People's Republic Of China; Corresponding author: jfhuang@mail.ntust.edu.tw


*Received 17 December 2008*


**ABSTRACT:** *A compact triple-band planar antenna applied to UMTS, WiFi and WiMAX applications is proposed. The proposed antenna provides three wide frequency bands, which are 1744–2759 MHz, 3271–4126 MHz and 4718–5908 MHz, realized in a commercial FR4 printed-circuit board (PCB) with a permittivity of 4.4 and thickness of 0.6 mm. Both simulation and measurement are pretty matched and indicate that the proposed antenna achieves gains to be 3.5, 3.0, and 2.5 dBi at 2.4, 3.5, and 5.2 GHz, respectively. The antenna dimension is 52.8 × 31.2 mm², smaller than presently published antennas discussed in comparison table.* © 2009 Wiley Periodicals, Inc. Microwave Opt Technol Lett 51: 2207–2212, 2009; Published online in Wiley InterScience (www.interscience.wiley.com). DOI 10.1002/mop.24522


**Key words:** *antenna; triple-band antenna; WiMAX; WiFi; UMTS; parasitical element*

## 1. INTRODUCTION

Modern communication requirements trendily keep on driving for wider bandwidth capabilities of antenna systems [1, 2]. The de-

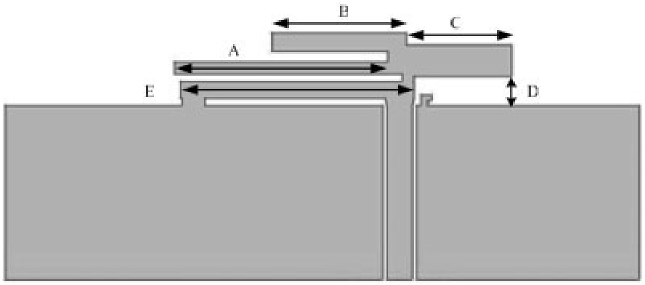


**Figure 1** Geometry of the triple-band printed planar antenna

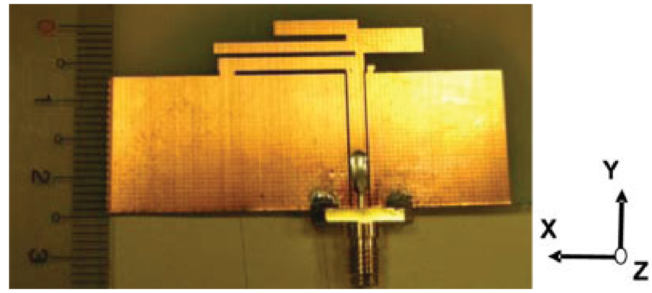


**Figure 2** Photograph of realized antenna. [Color figure can be viewed in the online issue, which is available at www.interscience.wiley.com]

signed antennas have to meet the latest technical requisitions for high speed data throughput and performance.

Typical characteristics like simplicity, lightweight, compact size, low profile, reliable manufacturability and wideband are as well as significant demands to take possession of more additional economic benefits. Printed coplanar waveguide (CPW) feed line architectures have been widely investigated in the previous literatures [3, 4] and are attractive for their conformability, easy implementation and cost effectiveness.

The dual-frequency planar antenna used in mobile handset is found in [5], but the frequency range only covers GSM900/1800. The bandwidth is not wide enough to cover WiMAX and 5.2 GHz ISM bands. Lots of researches have been carried out to improve antennas' bandwidth, and a number of different techniques have been discussed, including adding parasite patches, adopting multi-layer structures, using a thick air substrate, and adding a shorting post as reactive loading [6]. However, the bandwidth enhancement was achieved at the expense of over all efficiency. Hence, this article employed top loading method and two parasitical elements to achieve the bandwidth extension. This new type of antenna with simple structure, easy production and low cost is printed on 0.6 mm with relative permittivity 4.4 FR4 single-sided PCB bonded to CPW to achieve triple bands of 1744–2759 MHz, 3271–4126 MHz and 4718–5908 MHz. Field distributions are analyzed and verified by the useful IE3D simulation and measurement respectively.

## 2. DESIGN METHOD AND REALIZATION

Based on dipole methodology, by reducing the length of the dipole slightly shorter than half wavelength to resonate, the reactance can be reduced to zero, then the input impedance of the infinitely thin dipole, ignoring the skin effect, is about $70 + j0\ \Omega$, so the dipole resonant length practically must be slightly less than $\lambda/2$ where $\lambda$ is the wavelength in the medium.

It is also well known that the wire radius increases, the dipole must be shortened more to compensate the end effects and to obtain the same resonant frequency. The ends of the antenna are trimmed until a low value of standing wave ratio (VSWR) is obtained. As the length is reduced to obtain resonance, the input resistance also decreases and the reactance becomes zero. The thicker the dipole is, the wider bandwidth will be. Also, note that the minimum VSWR for the thicker dipole occurs at a lower frequency than for the thinner one.

**TABLE 1 Detail Dimension of Each Parameter in Figure 1**

| Parameter | Value |
|---|---|
| FR4 thickness | 0.6 mm |
| Permittivity ($\varepsilon_r$) | 4.4 |
| A | 22 mm |
| B | 14 mm |
| C | 5 mm |
| D | 3 mm |
| E | 23 mm |

The configuration of our first triple-band printed planar antenna is illustrated in Figure 1, which consists of a vertical strip and three asymmetric horizontal strips on the top that can produce three different surface current paths and result in three resonant modes.

This triple-band printed planar antenna was created by three elements of resonator and simulated by IE3D simulator. Variation value upon return loss (S11) by adding or reducing element A's length shows its tendency in different length and evidently indicates that the element A impacts 2.4 GHz a lot. It means 2 GHz band could be fine tuned by modifying the length of element A. Another 5.2 GHz band could be affected a little bit by element A as well. The other 3.5 GHz band is constantly unchanged, no matter what the element A changes.

With the same analytic method, the variation upon return loss (S11) by adding or reducing element B's length indicates that 3 GHz bands could be fine tuned. Results shown at 2.4 GHz and 5.2 GHz bands are more stable compared to 3.5 GHz band. Similarly, element C works on 5.2 GHz band which would be changed by modifying the length of element C.

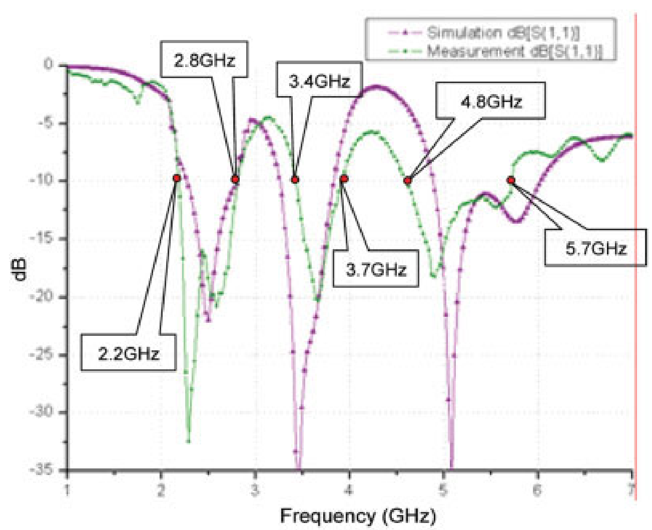


**Figure 3** Return loss between simulation and measurement. [Color figure can be viewed in the online issue, which is available at www.interscience.wiley.com]

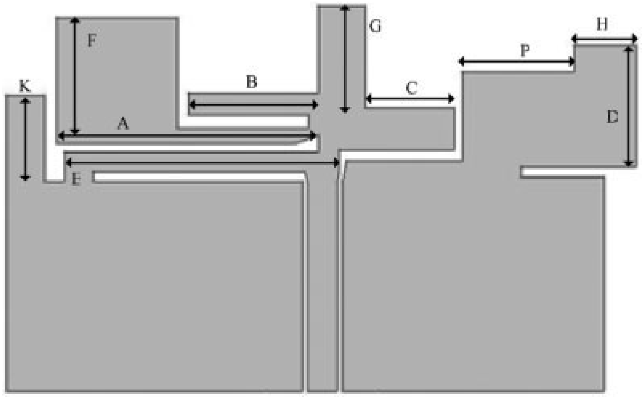


**Figure 4** Geometry of proposed antenna

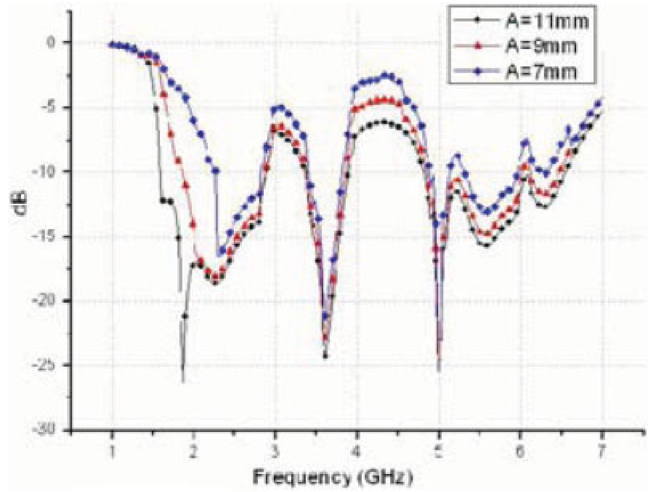


**Figure 6** Tuning dimensions of element A. [Color figure can be viewed in the online issue, which is available at www.interscience.wiley.com]

The detail size of each parameter in Figure 1 is shown in Table 1. Figure 2 illustrates a prototype of the triple-band printed planar antenna with a size of $62.2 \times 26.1$ mm$^2$. This planar antenna is very easy to implement in lots of portable devices.

The measured result compared with simulation data is shown in Figure 3. Measured results are commonly matched the simulated data. The measured bandwidth at 2.4 GHz band is wide very enough from 2.2 GHz to 2.8 GHz, and it is smaller than simulated data at 3.5 GHz band, but still meeting the requirement of WiMAX bands from 3.4 GHz to 3.7 GHz.

According to the measured results at 5.2 GHz band from 4.8 GHz to 5.7 GHz, it shows that just a little frequency shift happens. The reason for frequency shift may cause from the variation of FR4, based on the datasheet. FR4 is generally acceptable for signals up to around 3.5 GHz depending on applications. Loss and crosstalk will increase as the signal frequency increases, especially for the FR-4 board.

## 3. ADDING MORE ELEMENTS TO GET WIDER FREQUENCY BANDWIDTH

Based on the analysis of previous section, adding more resonators onto the antenna could get wider frequency bandwidth. Four radiating resonators with top loading method and two parasitical elements effectively extend wider bandwidth covering worldwide WiMAX and WiFi frequency bands. The dimensions of printed planar antenna are shown in Figure 4.

This proposed antenna is basically modified from Figure 1 antenna in which some elements are added to resonate multimodes to get wider frequency bandwidth.

Figure 5 shows the element A to be tuned from 7 mm to 11 mm.

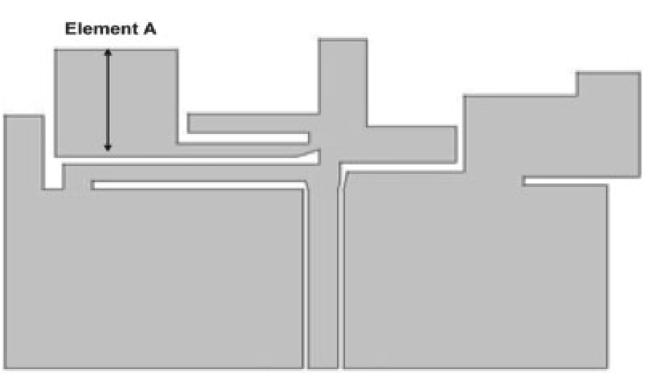


**Figure 5** Tuning dimension of element A

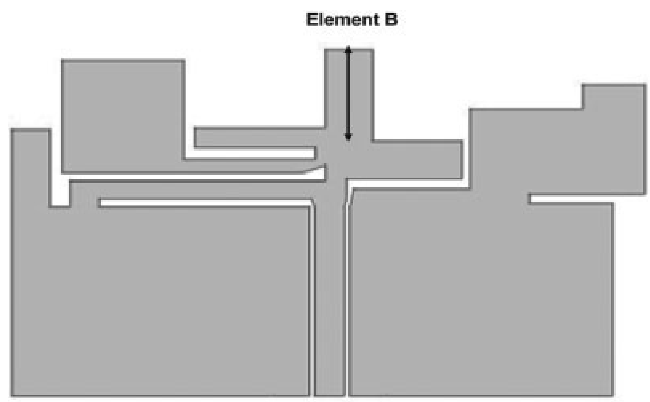


**Figure 7** Tuning dimensions of element B

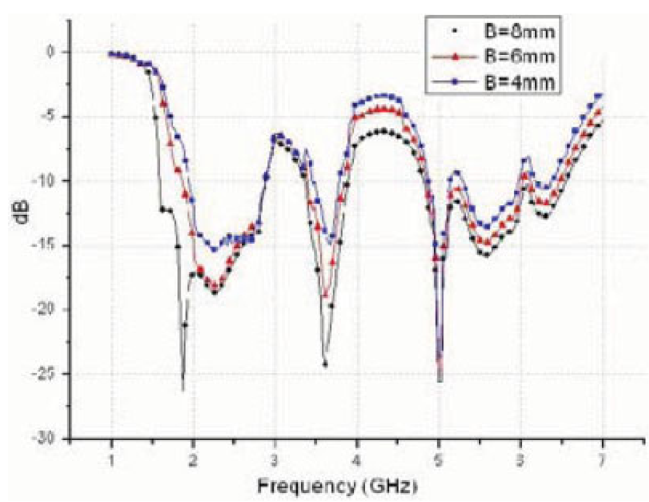


**Figure 8** Variation of return loss by modifying B's dimension. [Color figure can be viewed in the online issue, which is available at www.interscience.wiley.com]

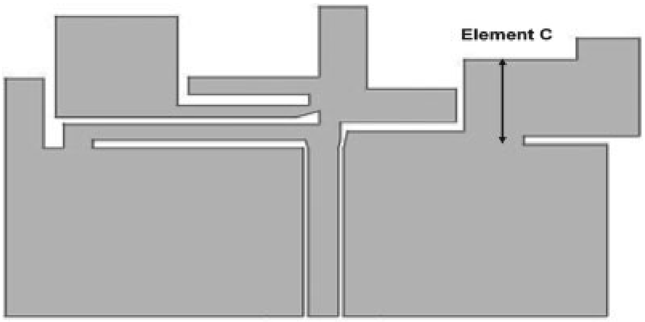


**Figure 9** Tuning dimension of element C

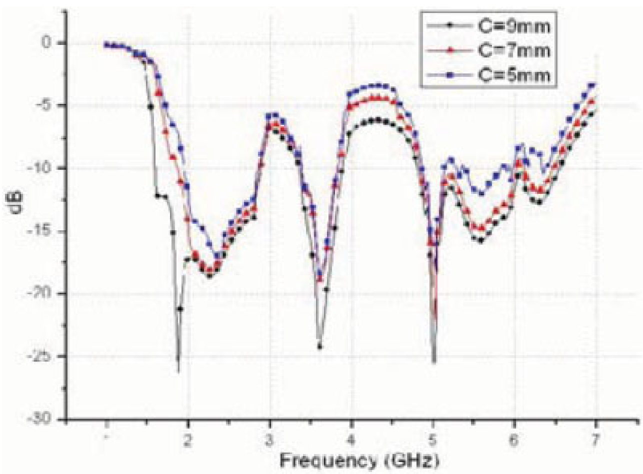


**Figure 10** Variation of return loss by modifying C's dimension. [Color figure can be viewed in the online issue, which is available at www.interscience.wiley.com]

As it can be seen, frequency bandwidth becomes wider in 2.4 GHz when it is 11 mm, the value chosen to carry out and implement for the paper. Figure 6 shows the curve of return loss with different A's dimensions tuned at 2.4 GHz band.

Similarly, Figure 7 shows the element B to be tuned from 8 mm to 4 mm. As it can be seen, return loss is lower in 3.5 GHz when it is 8 mm, the value chosen to carry out and implement for the paper. Figure 8 shows the curve of return loss with different B's dimensions tuned at 3.5 GHz band.

Actually the frequency bandwidth is wider than the antenna discussed in the previous section, because of adding more resonant elements. This method can be called top loading for enlarging the size of resonant elements.

Figure 9 shows the length of element C to be tuned from 5 mm to 9 mm, as it can be seen, return loss is lower at 5.5 GHz when

**TABLE 2 Dimension of Parameters Shown in Figure 4**

| Parameter | Value | Parameter | Value |
|---|---|---|---|
| PCB thickness | 0.6 mm | E | 23 mm |
| $\varepsilon_r$ | 4.4 | F | 10 mm |
| A | 22 mm | G | 8 mm |
| B | 11 mm | H | 5 mm |
| C | 7 mm | P | 9 mm |
| D | 10 mm | K | 7 mm |

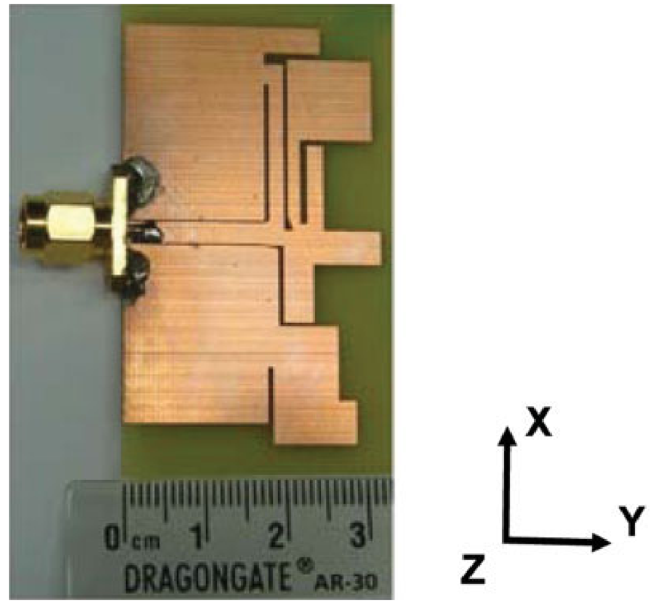


**Figure 11** Photograph of the proposed antenna. [Color figure can be viewed in the online issue, which is available at www.interscience.wiley.com]

element C is 9 mm. It is the value chosen to carry out and implement for the paper. Figure 10 shows the curve of return loss with different C's dimensions controlled at 5.2 GHz band.

The dimensions of printed planar antenna shown in Figure 4 are listed in Table 2. The photograph of the actual modified triple-band printed planar antenna is depicted in Figure 11 with 52.8 × 31.2 mm$^2$ dimension. It is very easy to be implemented in portable devices.

The return loss of simulation and measurement is shown in Figure 12. There are some differences between simulation and measurement. Both results prove that the antenna meets triple bands requirement operating at 2.4, 3.5, and 5.2 GHz, respectively. The first, second and third bands possess bandwidth nearly 1015(1744–2759) MHz,

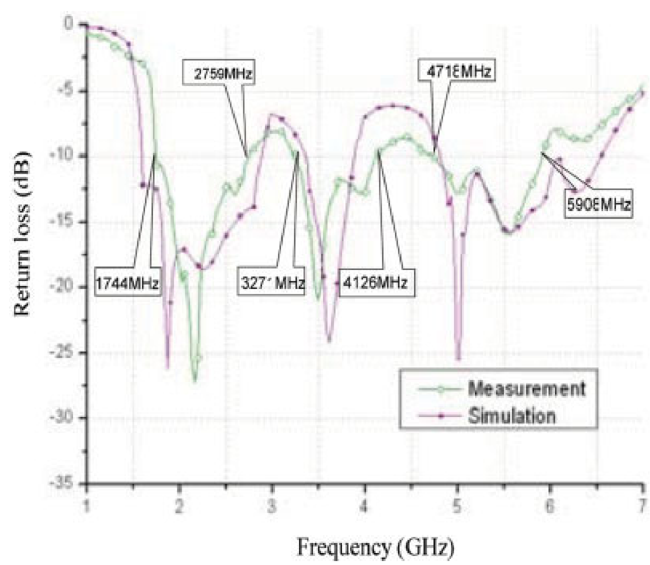


**Figure 12** Return loss of simulation and measurement. [Color figure can be viewed in the online issue, which is available at www.interscience.wiley.com]

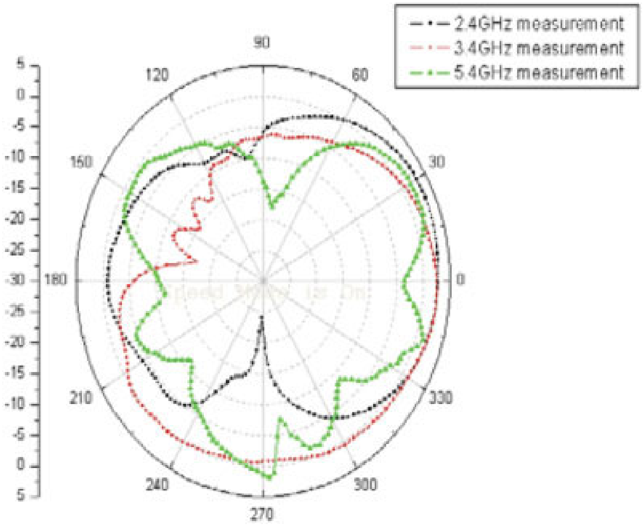


**Figure 13** Radiation pattern at XY plane. [Color figure can be viewed in the online issue, which is available at www.interscience.wiley.com]

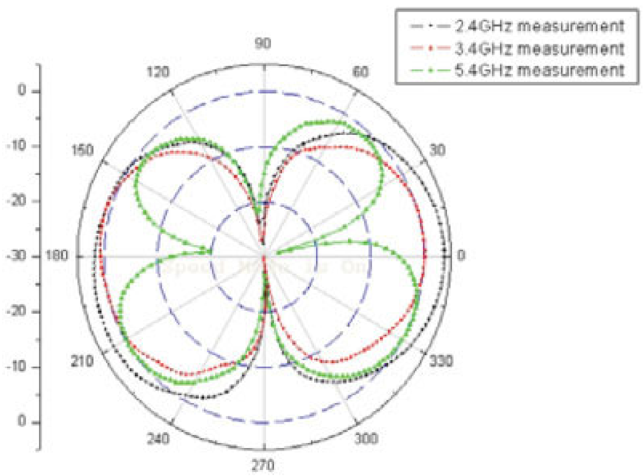


**Figure 14** Radiation pattern at YZ plane. [Color figure can be viewed in the online issue, which is available at www.interscience.wiley.com]

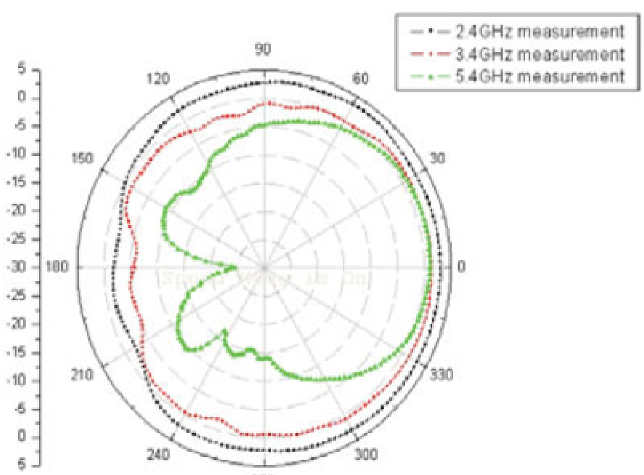


**Figure 15** Radiation pattern at XZ plane. [Color figure can be viewed in the online issue, which is available at www.interscience.wiley.com]

**TABLE 3 Summary of Comparison Table**

| Antenna parameters | | Ref [9] | Ref [10] | This work |
|---|---|---|---|---|
| 2500 MH | $f_L$(MHz) | 1660 | 2128 | 1744 |
| z band | $f_U$(MHz) | 2590 | 2769 | 2759 |
| | BW(MHz) | 930 | 641 | 1029 |
| 3500 MH | $f_L$(MHz) | NA | 2941 | 3271 |
| z band | $f_U$(MHz) | NA | 3809 | 4126 |
| | BW(MHz) | NA | 868 | 855 |
| 5500 MH | $f_L$(MHz) | 4480 | 4590 | 4718 |
| z band | $f_U$(MHz) | 5890 | 6601 | 5908 |
| | BW(MHz) | 1410 | 2011 | 1190 |
| Size | (mm × mm) | 54 × 50 | 61 × 50 | 31.2 × 52.8 |

855(3271–4126) MHz and 1190(4718–5908) MHz, respectively. The bandwidth has remarkably improved by adding some parasitic components to get better matching.

Measured radiation patterns in XY, YZ and XZ planes are shown in Figures 13, 14, and 15 respectively. Radiation patterns are in pretty good performance and cover the triple band frequency ranges. Figures 13 to 15 indicate the proposed antenna achieves gains to be 3.5, 3.0, and 2.5 dBi at 2.4, 3.4, and 5.4 GHz respectively. Both of them present good performance in both low band and high band and approach approximately omnidirectional radiation characteristics, which can be implemented to portable devices.

Table 3 gives a comparison table upon related papers for comparing performances of WiMAX antenna, in which the proposed antenna has larger bandwidth than other types of antenna.

In [7, 8], the T-shaped monopole is with a notch fed by microstrip line, but our antenna is fed by CPW. Actually, four radiating resonators with top loading method and two parasitical elements effectively extend wider bandwidth covering worldwide UMTS, WiFi and WiMAX frequency bands.

In addition, the proposed antenna has the smallest size compared to the reference antennas, and it is very suitable for implementing in portable devices.

## 4. CONCLUSIONS

Our antenna has been verified in good agreement by measurement and simulation. Measurement shows that the antenna gain is 3.5 dB for 2.4 GHz band, 3.0 dB for 3.5 GHz band and 2.5 dB for 5.2 GHz band, respectively. Also, the 3 dB passband widths are about 1015(1744–2759) MHz, 855(3271–4126) MHz and 1190(4718–5908) MHz, respectively. The antenna dimension is 52.8 × 31.2 × 0.6 $mm^3$, smaller than presently published antennas discussed in this article. Both characteristics of the broad band and compact dimension make the proposed antenna very suitable for the UMTS, WLAN and WiMAX applications.

## REFERENCES

1. B.G. Duffley, G.A. Morin, M. Mikavica, and Y.M.M. Antar, A wideband printed double-sided dipole array, IEEE Trans Antennas Propagat 52 (2004), 628–631.
2. S. Dey, P. Venugopalan, K.A. Jose, C.K. Anandan, P. Mohanan, and K.G. Nair, Bandwidth enhancement by flared microstrip dipole antenna, Antennas and Propagation Society International Symposium, 1991 AP-S Digest 1 (1991), 342–345.
3. K.F. Tong, K. Li, T. Matsui, and M. Izutsu, Wideband coplanar waveguide fed coplanar patch antenna, Antennas and Propagation Society International Symposium, 2001. IEEE 3 (2001), 406–409.
4. W. Wilkinson, A class of printed circuit antennas, IEEE Antennas Propagat Symp Dig (1974), 270–274.
5. P.L. Teng, T.W. Chiou, and K.L. Wong, Planar inverted-F antenna

with a bent, meandered radiating arm for GSM/DCS operation, Microwave Opt Technol Lett 38 (2003), 73–75.
6. K.-L. Wong, L.-C. Chou, and C.-M. Su, Dual-band flat-plate antenna with a shorted parasitic element for laptop applications, IEEE Trans Antennas Propagat 53 (2005), 539–544.
7. S.-B. Chen, Y.-C. Jaio, W.-W., and F.-S. Zhang, Modified T-shaped planar monopole antennas for multiband operation, IEEE Trans Microwave Theory Technol 54 (2006), 3267–3270.
8. J.-F. Huang and S.-H. Wu, Planar T- shaped monopole antenna for WLAN/WiMAX applications, IEICE Trans Electron E91-C (2008), 625–630.
9. X.C. Lin, L.T. Wang, C.L. Lai, and Y.S. Liu, A broadband CPW-fed inductive slot antenna, Microwave Opt Technol Lett 41 (2004), 12–14.
10. R. Chair, A.A. Kishk, and K.F. Lee, Ultrawide-band coplanar waveguide-fed rectangular slot antenna, IEEE Antennas Wireless Propagat Lett 3 (2004), 227–229.



# MULTIBAND NOTEBOOK COMPUTER ANTENNA DESIGN BY FDTD METHOD FOR GSM/WCDMA SYSTEM APPLICATIONS

**Jhin-Fang Huang, Jiun-Yu Wen, and Sheng-Chih Lin**
Department of Electronic Engineering, National Taiwan University of Science and Technology, No. 43, Kee-Lung Rd. Sec. 4, Taipei 10672, Taiwan, Republic of China; Corresponding author: jfhuang@mail.ntust.edu.tw

*Received 17 December 2008*

**ABSTRACT:** *In this study, a simple structure designed antenna for 2G and 3G mobile communication applied to notebook computer (NB) is proposed and analyzed by finite difference time domain (FDTD). The proposed antenna has great characteristics of simple structure, easy production, low cost, good impedance matching, and wideband frequency. The antenna main structure is printed on 0.8 mm with permittivity 4.4 FR4 single-sided PCB, which is bonded to metal bracket. This proposed antenna covers GSM 850/900/1800/1900 and WCDMA multi-bands and satisfies NB wireless wide area network system. Both FDTD simulation and measurement show that the antenna gain is 2.2 dB for 800 MHz band and 4.6 dB for 1800 MHz band. The 3-dB passbands are about 136 (824–960 MHz) and 460 MHz (1710–2170 MHz), respectively. The bandwidth of each passband is matched with the desirable values for the NB multiband requirement.* © 2009 Wiley Periodicals, Inc. Microwave Opt Technol Lett 51: 2212–2216, 2009; Published online in Wiley InterScience (www.interscience.wiley.com). DOI 10.1002/mop.24521

**Key words:** *multiband antenna; WCDMA; WLAN; WWAN; wireless wide area network*

## 1. INTRODUCTION

For fast flourishing development on mobile communication, dual-band and triband antenna designs could no longer satisfy market demands. Design approach does not only focus on minimizing physical size but also cover more and more wide band frequencies in very limited space available. The size must be thin, short, and small. The weight also must be light.

After Centrino populates the wireless location area network (WLAN) market, Intel is doing well to promote and combine the future NB concepts with wireless wide area network (WWAN) for mobile communication in NB as well. Actually, a NB today will have both WLAN and WWAN functions built embedded.

It is well known that WWAN includes four bands (GSM850/900/1800/1900), which are allocated in the mobile communication system. To combine four GSM bands and WCDMA in antenna design for mobile, cellular phone requires large space for antenna to cover the all required frequencies. But in practical situation, it is necessary to keep the mobile phone in portable and minimizing size. Recently, there are many literatures of UWB antennas used in mobile communications [1–3], but the problem is that their sizes are not small enough to satisfy the limited mechanism of NB. Also, their calculation did not concern too much about the surrounded space of the antenna. The dual-frequency planar antenna used in a mobile handset is found in [4], but the frequency range only covers GSM900/1800. The bandwidth is not wide enough to cover WCDMA band. Therefore, in this study, we propose a new type of loop antenna with simple structure, easy production, and low cost. The antenna main structure is printed on 0.8 mm with relative permittivity 4.4 FR4 single-sided PCB bonded to metal bracket to achieve dual modes containing all bands of GSM 850/900/1800/1900 and WCDMA. Its size is minimized and suitable for this WWAN antenna to build embedded. Field distributions are analyzed and verified by the useful simulator finite difference time domain (FDTD) and measurement, respectively.

## 2. FDTD PRINCIPLE

### *2.1. Finite Difference Approximation of Maxwell's Equations*

The discussed numerical method, FDTD, a time-domain approach was first treated by Yee [5] to deal with electromagnetic field distributions. Through the work of Yee, FDTD has become a powerful tool in predicting scattering problems. Two workers found the applications of FDTD in transient electromagnetics [6], [7]. One calculated the distant scattered field in back direction, and the other was interested in the distant refracted field in an unlimited space. All of them did not account for the field propagation much about surrounded obstacle shape. Therefore, we apply this method to analyze the designed antenna in a limited and irregular space, especially in a NB.

A transceiver antenna must satisfy Maxwell's curl equations.

$$\nabla \times \bar{H} = \varepsilon \frac{\partial \bar{E}}{\partial t} \tag{1}$$

$$\nabla \times \bar{E} = -\mu \frac{\partial \bar{H}}{\partial t}, \tag{2}$$

where $\varepsilon$ and $\mu$ are the medium permittivity and permeability, respectively.

Follow Yee's suggestion and denote the function of space and time as:

$$F^n(i,j,k) = F(i\Delta x, j\Delta y, k\Delta z, n\Delta t), \tag{3}$$

where $\Delta t$ is the time increment and $n$ denotes the $n$th-time step.

The FDTD approach proceeds to solve for the electric and magnetic fields resulting from a radiating wave interacting with the radiator by dividing both time and space into a numerical grids. Figure 1 illustrates the grid points of the electric and magnetic field components about a unit cell of the FDTD lattice in Cartesian coordinates. It should be noted that each electric field component is surrounded by four circulating magnetic components and vice versa. With each cell, six components of the electric and magnetic fields are computed successively and alternatively at different points in time steps. It is also noted that electric and magnetic

# 射 频 和 天 线 设 计 培 训 课 程 推 荐

易迪拓培训(www.edatop.com)由数名来自于研发第一线的资深工程师发起成立，致力并专注于微波、射频、天线设计研发人才的培养；我们于 2006 年整合合并微波 EDA 网(www.mweda.com)，现已发展成为国内最大的微波射频和天线设计人才培养基地，成功推出多套微波射频以及天线设计经典培训课程和 ADS、HFSS 等专业软件使用培训课程，广受客户好评；并先后与人民邮电出版社、电子工业出版社合作出版了多本专业图书，帮助数万名工程师提升了专业技术能力。客户遍布中兴通讯、研通高频、埃威航电、国人通信等多家国内知名公司，以及台湾工业技术研究院、永业科技、全一电子等多家台湾地区企业。

易迪拓培训课程列表：http://www.edatop.com/peixun/rfe/129.html


## 射频工程师养成培训课程套装

该套装精选了射频专业基础培训课程、射频仿真设计培训课程和射频电路测量培训课程三个类别共 30 门视频培训课程和 3 本图书教材；旨在引领学员全面学习一个射频工程师需要熟悉、理解和掌握的专业知识和研发设计能力。通过套装的学习，能够让学员完全达到和胜任一个合格的射频工程师的要求…

课程网址：http://www.edatop.com/peixun/rfe/110.html

## ADS 学习培训课程套装

该套装是迄今国内最全面、最权威的 ADS 培训教程，共包含 10 门 ADS 学习培训课程。课程是由具有多年 ADS 使用经验的微波射频与通信系统设计领域资深专家讲解，并多结合设计实例，由浅入深、详细而又全面地讲解了 ADS 在微波射频电路设计、通信系统设计和电磁仿真设计方面的内容。能让您在最短的时间内学会使用 ADS，迅速提升个人技术能力，把 ADS 真正应用到实际研发工作中去，成为 ADS 设计专家...

课程网址： http://www.edatop.com/peixun/ads/13.html

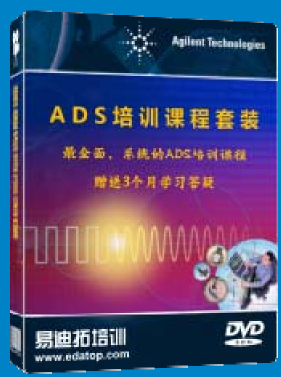



## HFSS 学习培训课程套装

该套课程套装包含了本站全部 HFSS 培训课程，是迄今国内最全面、最专业的 HFSS 培训教程套装，可以帮助您从零开始，全面深入学习 HFSS 的各项功能和在多个方面的工程应用。购买套装，更可超值赠送 3 个月免费学习答疑，随时解答您学习过程中遇到的棘手问题，让您的 HFSS 学习更加轻松顺畅…

课程网址：http://www.edatop.com/peixun/hfss/11.html

## CST 学习培训课程套装

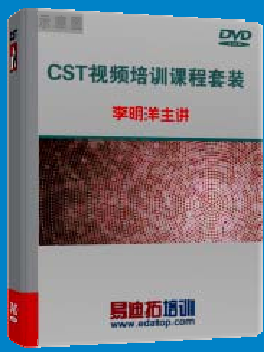


该培训套装由易迪拓培训联合微波 EDA 网共同推出，是最全面、系统、专业的 CST 微波工作室培训课程套装，所有课程都由经验丰富的专家授课，视频教学，可以帮助您从零开始，全面系统地学习 CST 微波工作的各项功能及其在微波射频、天线设计等领域的设计应用。且购买该套装，还可超值赠送 3 个月免费学习答疑…

课程网址：http://www.edatop.com/peixun/cst/24.html


## HFSS 天线设计培训课程套装

套装包含 6 门视频课程和 1 本图书，课程从基础讲起，内容由浅入深，理论介绍和实际操作讲解相结合，全面系统的讲解了 HFSS 天线设计的全过程。是国内最全面、最专业的 HFSS 天线设计课程，可以帮助您快速学习掌握如何使用 HFSS 设计天线，让天线设计不再难…

课程网址：http://www.edatop.com/peixun/hfss/122.html

## 13.56MHz NFC/RFID 线圈天线设计培训课程套装


套装包含 4 门视频培训课程，培训将 13.56MHz 线圈天线设计原理和仿真设计实践相结合，全面系统地讲解了 13.56MHz 线圈天线的工作原理、设计方法、设计考量以及使用 HFSS 和 CST 仿真分析线圈天线的具体操作，同时还介绍了 13.56MHz 线圈天线匹配电路的设计和调试。通过该套课程的学习，可以帮助您快速学习掌握 13.56MHz 线圈天线及其匹配电路的原理、设计和调试…

详情浏览：http://www.edatop.com/peixun/antenna/116.html

## 我们的课程优势：

※ 成立于 2004 年，10 多年丰富的行业经验，

※ 一直致力并专注于微波射频和天线设计工程师的培养，更了解该行业对人才的要求

※ 经验丰富的一线资深工程师讲授，结合实际工程案例，直观、实用、易学

## 联系我们：

※ 易迪拓培训官网：http://www.edatop.com

※ 微波 EDA 网：http://www.mweda.com

※ 官方淘宝店：http://shop36920890.taobao.com